Supporting Information

Phase Transition Model of Ferroelectric 2D Hybrid Perovskites

Andrius Ibenskas,[†] Daria Szewczyk,[‡] Mirosław Mączka,[‡] Jūras Banys,[¶] Evaldas E. Tornau,[†] and Mantas Šimėnas[*,¶]

[†]*Center for Physical Sciences and Technology, Sauletekio 3, LT-10257 Vilnius, Lithuania*

[‡]*Institute of Low Temperature and Structure Research, Polish Academy of Sciences, Okólna 2, PL-50-422 Wroclaw, Poland*

[¶]*Faculty of Physics, Vilnius University, Sauletekio 3, LT-10257 Vilnius, Lithuania*

E-mail: mantas.simenas@ff.vu.lt

Additional model details

All MA-MA, MA-BA, and BA-BA interactions included in our model are illustrated in Figures S1-S3.

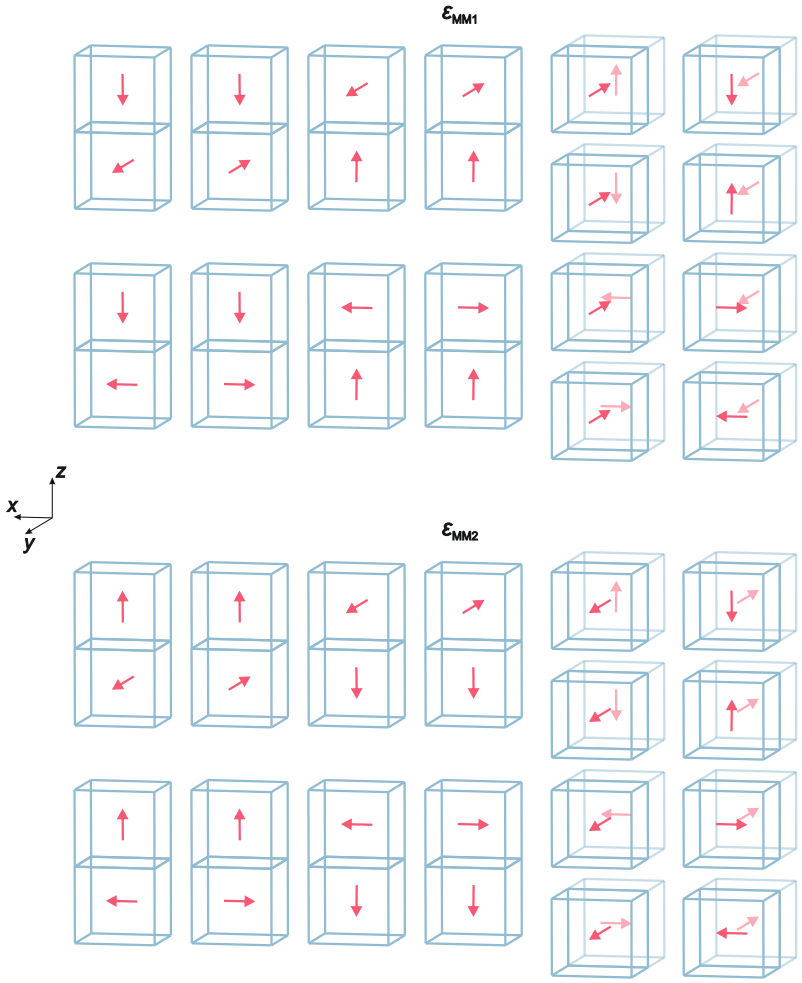

Figure S1: MA-MA type interactions considered in our model.

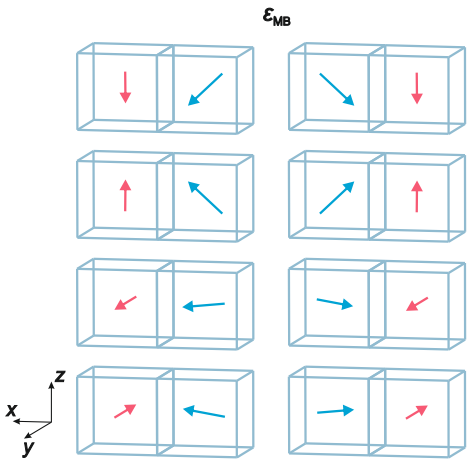

Figure S2: MA-BA type interactions considered in our model.

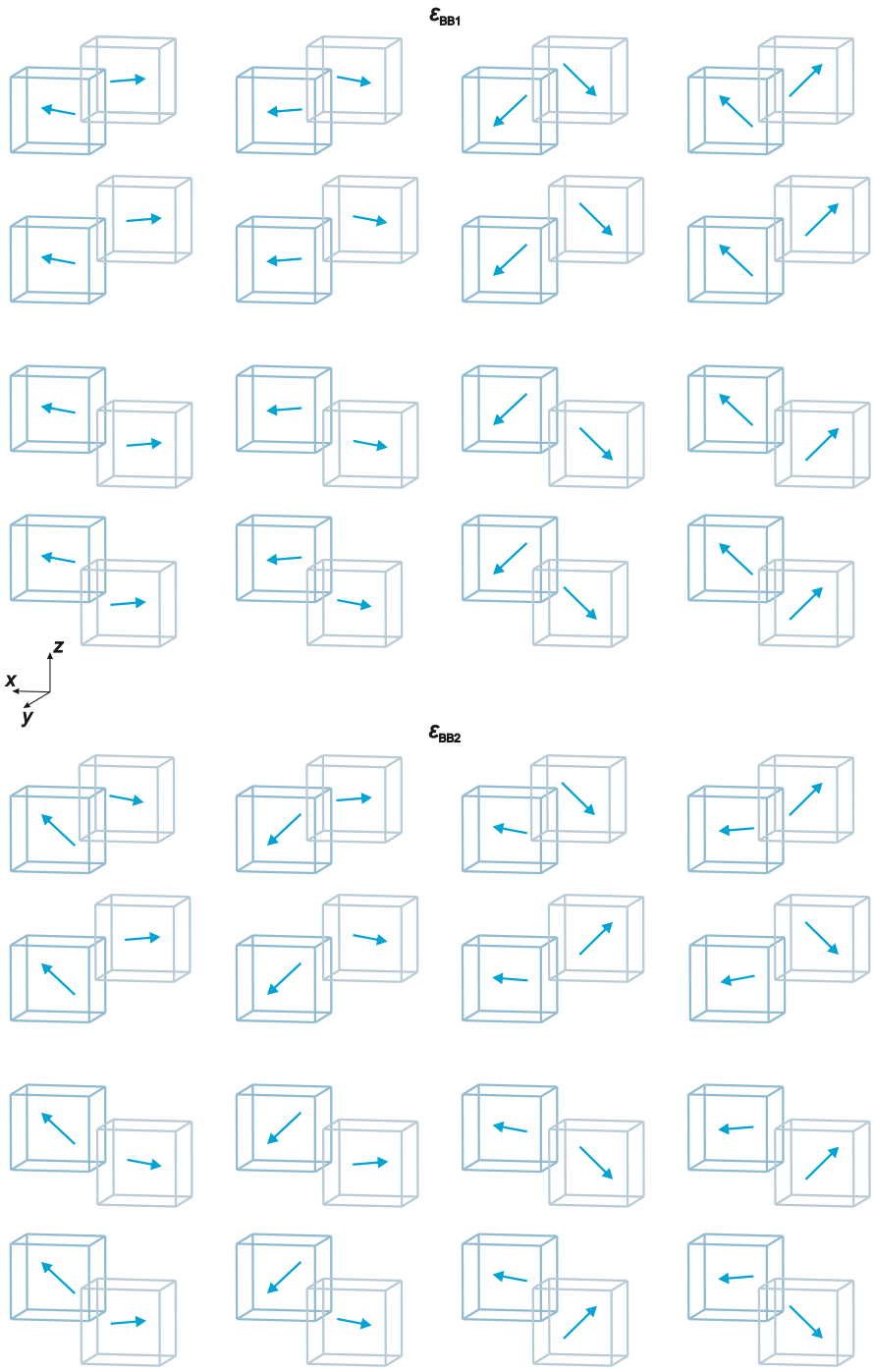

Figure S3: BA-BA type interactions considered in our model.

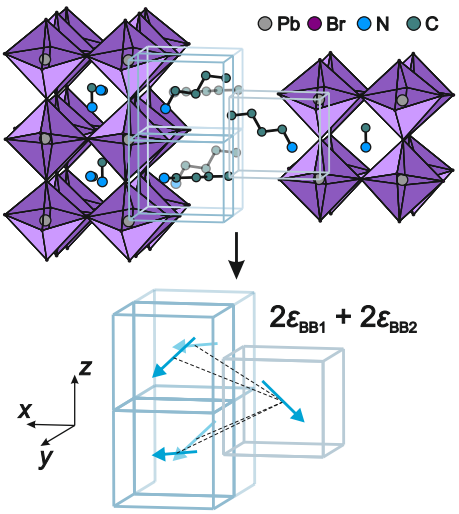

Figure S4: Mapping of the BA sublattice onto the model lattice. Each BA cation interacts with four BA cations located in the adjacent plane.

The effective Hamiltonian describing the MA-MA interactions can be expressed as

$$\mathcal{H}_{\mathrm{MM}} = \mathcal{H}_{\mathrm{MM1}} + \mathcal{H}_{\mathrm{MM2}}, \tag{S1}$$

where

$$\begin{aligned}\mathcal{H}_{\mathrm{MM1}} = -\varepsilon_{\mathrm{MM1}} \sum_{<ij>} \Big\{ & \delta(S_i^{\mathrm{M}},1)\Big[\delta_{+z}(S_j^{\mathrm{M}},2) + \delta_{+z}(S_j^{\mathrm{M}},3) + \delta_{+z}(S_j^{\mathrm{M}},5) + \delta_{+z}(S_j^{\mathrm{M}},6)\Big] \\ & + \delta(S_i^{\mathrm{M}},2)\Big[\delta_{-y}(S_j^{\mathrm{M}},1) + \delta_{-y}(S_j^{\mathrm{M}},3) + \delta_{-y}(S_j^{\mathrm{M}},4) + \delta_{-y}(S_j^{\mathrm{M}},6)\Big] \\ & + \delta(S_i^{\mathrm{M}},4)\Big[\delta_{-z}(S_j^{\mathrm{M}},2) + \delta_{-z}(S_j^{\mathrm{M}},3) + \delta_{-z}(S_j^{\mathrm{M}},5) + \delta_{-z}(S_j^{\mathrm{M}},6)\Big] \\ & + \delta(S_i^{\mathrm{M}},5)\Big[\delta_{+y}(S_j^{\mathrm{M}},1) + \delta_{+y}(S_j^{\mathrm{M}},3) + \delta_{+y}(S_j^{\mathrm{M}},4) + \delta_{+y}(S_j^{\mathrm{M}},6)\Big]\Big\},\end{aligned} \tag{S2}$$

and

$$\mathcal{H}_{\mathrm{MM2}} = -\varepsilon_{\mathrm{MM2}} \sum_{<ij>} \Big\{ \delta(S_i^{\mathrm{M}},1)\Big[\delta_{-z}(S_j^{\mathrm{M}},2) + \delta_{-z}(S_j^{\mathrm{M}},3) + \delta_{-z}(S_j^{\mathrm{M}},5) + \delta_{-z}(S_j^{\mathrm{M}},6)\Big] + \delta(S_i^{\mathrm{M}},2)\Big[\delta_{+y}(S_j^{\mathrm{M}},1) + \delta_{+y}(S_j^{\mathrm{M}},3) + \delta_{+y}(S_j^{\mathrm{M}},4) + \delta_{+y}(S_j^{\mathrm{M}},6)\Big] + \delta(S_i^{\mathrm{M}},4)\Big[\delta_{+z}(S_j^{\mathrm{M}},2) + \delta_{+z}(S_j^{\mathrm{M}},3) + \delta_{+z}(S_j^{\mathrm{M}},5) + \delta_{+z}(S_j^{\mathrm{M}},6)\Big] + \delta(S_i^{\mathrm{M}},5)\Big[\delta_{-y}(S_j^{\mathrm{M}},1) + \delta_{-y}(S_j^{\mathrm{M}},3) + \delta_{-y}(S_j^{\mathrm{M}},4) + \delta_{-y}(S_j^{\mathrm{M}},6)\Big]\Big\}. \tag{S3}$$

Here, $\delta(m,n)$ denotes the Kronecker delta, which equals one when $m = n$ and zero otherwise. The indices i and j enumerate the sites of the cubic lattice in our mode, while the summation excludes double counting and takes into account only the pairs listed in Figure S1.

Analogously, the effective Hamiltonians for the MA-BA and BA-BA interactions are defined below.

$$\mathcal{H}_{\mathrm{MB}} = -\varepsilon_{\mathrm{MB}} \sum_{<ij>} \Big\{ \delta(S_i^{\mathrm{M}},1)\Big[\delta_{+x}(S_j^{\mathrm{B}},1) + \delta_{-x}(S_j^{\mathrm{B}},8)\Big] + \delta(S_i^{\mathrm{M}},2)\Big[\delta_{+x}(S_j^{\mathrm{B}},2) + \delta_{-x}(S_j^{\mathrm{B}},7)\Big] + \delta(S_i^{\mathrm{M}},4)\Big[\delta_{+x}(S_j^{\mathrm{B}},4) + \delta_{-x}(S_j^{\mathrm{B}},5)\Big] + \delta(S_i^{\mathrm{M}},5)\Big[\delta_{+x}(S_j^{\mathrm{B}},3) + \delta_{-x}(S_j^{\mathrm{B}},6)\Big]\Big\}. \tag{S4}$$

$$\mathcal{H}_{\mathrm{BB}} = \mathcal{H}_{\mathrm{BB1}} + \mathcal{H}_{\mathrm{BB2}}, \tag{S5}$$

where

$$\mathcal{H}_{\mathrm{BB1}} = -\varepsilon_{\mathrm{BB1}} \sum_{<ij>} \Big\{ \delta(S_i^{\mathrm{B}},1)\Big[\delta_{+x,-y,-z}(S_j^{\mathrm{B}},8) + \delta_{+x,+y,-z}(S_j^{\mathrm{B}},8) + \delta_{+x,+y,+z}(S_j^{\mathrm{B}},8) + \delta_{+x,-y,+z}(S_j^{\mathrm{B}},8)\Big] + \delta(S_i^{\mathrm{B}},2)\Big[\delta_{+x,-y,-z}(S_j^{\mathrm{B}},7) + \delta_{+x,+y,-z}(S_j^{\mathrm{B}},7) + \delta_{+x,+y,+z}(S_j^{\mathrm{B}},7) + \delta_{+x,-y,+z}(S_j^{\mathrm{B}},7)\Big] + \delta(S_i^{\mathrm{B}},3)\Big[\delta_{+x,-y,-z}(S_j^{\mathrm{B}},6) + \delta_{+x,+y,-z}(S_j^{\mathrm{B}},6) + \delta_{+x,+y,+z}(S_j^{\mathrm{B}},6) + \delta_{+x,-y,+z}(S_j^{\mathrm{B}},6)\Big] + \delta(S_i^{\mathrm{B}},4)\Big[\delta_{+x,-y,-z}(S_j^{\mathrm{B}},5) + \delta_{+x,+y,-z}(S_j^{\mathrm{B}},5) + \delta_{+x,+y,+z}(S_j^{\mathrm{B}},5) + \delta_{+x,-y,+z}(S_j^{\mathrm{B}},5)\Big]\Big\}, \tag{S6}$$

and

$$\mathcal{H}_{\mathrm{BB2}} = -\varepsilon_{\mathrm{BB2}} \sum_{<ij>} \Big\{ \delta(S_i^{\mathrm{B}},1)\Big[\delta_{+x,-y,-z}(S_j^{\mathrm{B}},6) + \delta_{+x,+y,-z}(S_j^{\mathrm{B}},7) + \delta_{+x,+y,+z}(S_j^{\mathrm{B}},6) + \delta_{+x,-y,+z}(S_j^{\mathrm{B}},7)\Big] + \delta(S_i^{\mathrm{B}},2)\Big[\delta_{+x,-y,-z}(S_j^{\mathrm{B}},5) + \delta_{+x,+y,+z}(S_j^{\mathrm{B}},5) + \delta_{+x,+y,-z}(S_j^{\mathrm{B}},8) + \delta_{+x,-y,+z}(S_j^{\mathrm{B}},8)\Big] + \delta(S_i^{\mathrm{B}},3)\Big[\delta_{+x,+y,-z}(S_j^{\mathrm{B}},5) + \delta_{+x,-y,+z}(S_j^{\mathrm{B}},5) + \delta_{+x,+y,+z}(S_j^{\mathrm{B}},8) + \delta_{+x,-y,-z}(S_j^{\mathrm{B}},8)\Big] + \delta(S_i^{\mathrm{B}},4)\Big[\delta_{+x,-y,-z}(S_j^{\mathrm{B}},7) + \delta_{+x,+y,-z}(S_j^{\mathrm{B}},6) + \delta_{+x,+y,+z}(S_j^{\mathrm{B}},7) + \delta_{+x,-y,+z}(S_j^{\mathrm{B}},6)\Big] \Big\}. \tag{S7}$$

Additional simulation results

Snapshots obtained in the two-transition region of the phase diagram for $\varepsilon_{\mathrm{BB1}} = \varepsilon_{\mathrm{BB2}} = \varepsilon_{\mathrm{BB}}$ are presented in Figure S5 showing a similar disordered cation arrangement in the HT phase. In the intermediate phase, orientational order emerges within the MA sublattice, but correlations between adjacent perovskite slabs remain weak due to the small $\varepsilon_{\mathrm{BB}}$ coupling. Consequently, the higher-temperature transition corresponds to the onset of MA cation ordering, whereas the lower-temperature transition is associated with the ordering of BA cations and the coupling between MA slabs. However, a long-range order is only partially achieved, as the BA cations are unable to fully adapt to the incommensurate MA arrangements in neighboring slabs.

For the case of $|\varepsilon_{\mathrm{BB1}}| > |\varepsilon_{\mathrm{BB2}}|$ and $\varepsilon_{\mathrm{BB1}}/\varepsilon_{\mathrm{MM1}} \gtrsim 0.7$, the phase transition sequence is reversed. As a result, the intermediate phase is characterized by partial ordering of the BA sublattice, which also induces a degree of ordering in the MA cations, although the MA sublattice remains largely disordered in the yz-plane (Figure S6).

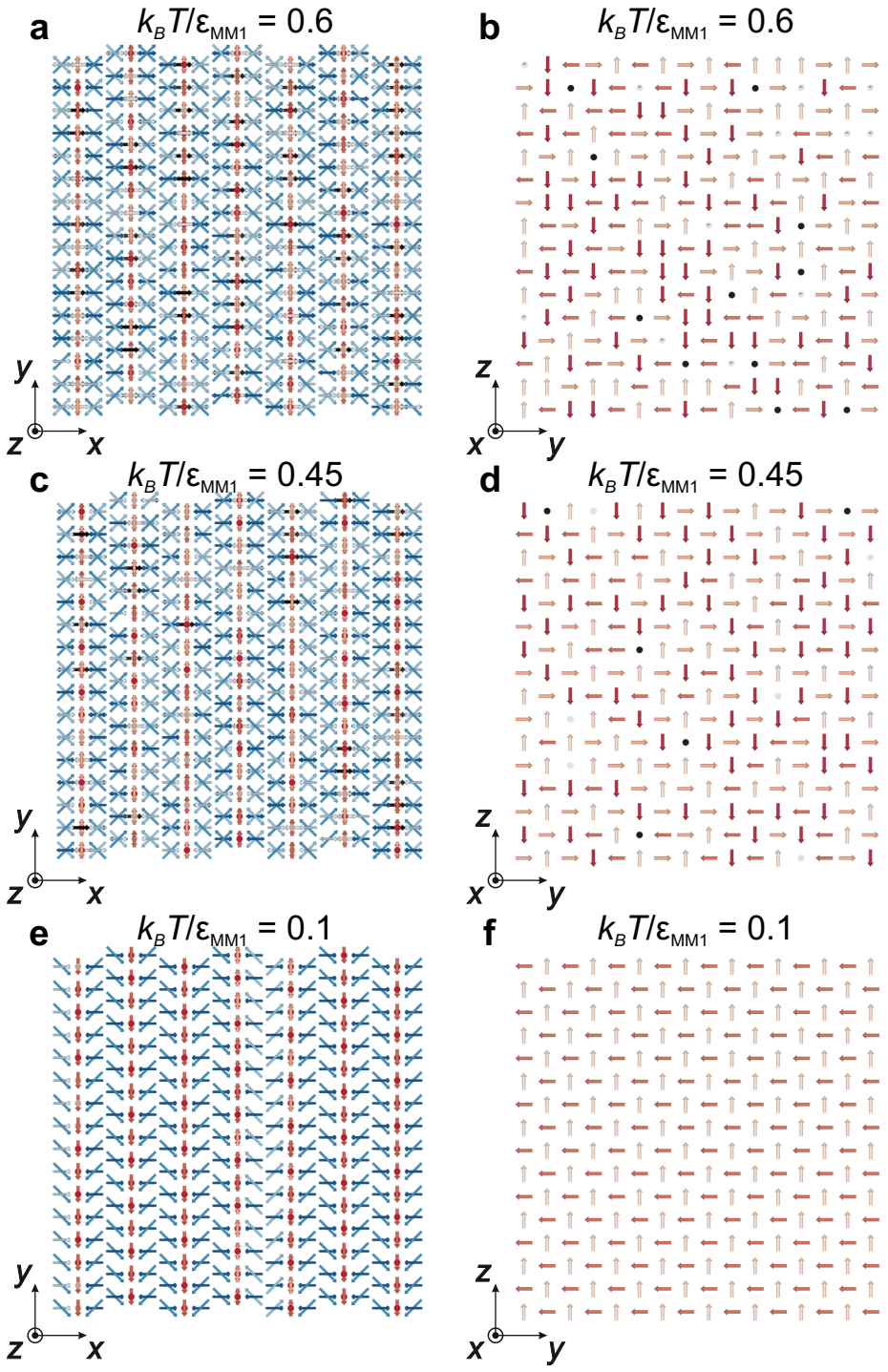

Figure S5: Snapshots of MA (red) and BA (blue) cation arrangements (a,b) in the disordered phase ($k_BT/\varepsilon_{\mathrm{MM1}} = 0.6$), (c,d) partially ordered phase ($k_BT/\varepsilon_{\mathrm{MM1}} = 0.45$), and (e,f) LT phase ($k_BT/\varepsilon_{\mathrm{MM1}} = 0.1$) as obtained by MC simulations of our model for $\varepsilon_{\mathrm{MB}}/\varepsilon_{\mathrm{MM1}} = 0.6$ and $\varepsilon_{\mathrm{BB}}/\varepsilon_{\mathrm{MM1}} = 0.4$. View along the (a,c,e) z-axis (multiple MA and BA layers) and (b,d,f) x-axis (single MA slab).

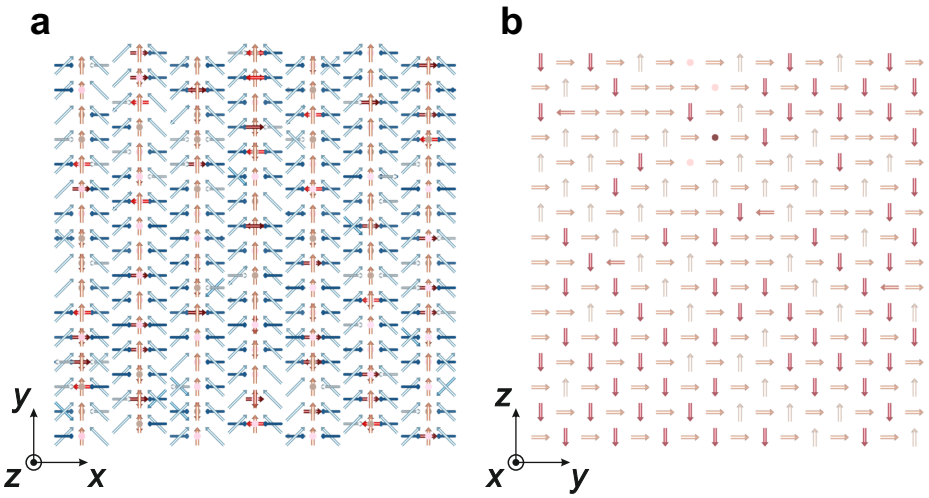

Figure S6: Snapshots of MA (red) and BA (blue) cation arrangements (a,b) in the intermediate phase as obtained by MC simulations of our model for $\varepsilon_{\mathrm{BB1}}/\varepsilon_{\mathrm{BB2}} = 2$, $\varepsilon_{\mathrm{MB}}/\varepsilon_{\mathrm{MM1}} = 0.95$, and $\varepsilon_{\mathrm{BB1}}/\varepsilon_{\mathrm{MM1}} = 0.8$. View along the (a) z-axis (multiple MA and BA layers) and (b) x-axis (single MA slab).